COMPOSITES WITH SIMULTANEOUS VIBRATION CONTROL, ENERGY HARVESTING AND SELF-SENSING CAPABILITIES

Y. Wang[1] and D. J. Inman[2*]
[1]Department of Mechanical Engineering, Virginia Tech, Blacksburg, VA 24061, USA
[2]Department of Aerospace Engineering, University of Michigan, Ann Arbor, MI 48109, USA
[*]Corresponding Author (DanInman@umich.edu)

Keywords: *Composites, Energy Harvesting, Self-sensing, Simultaneous Control*

1 Introduction

Multifunctional structures hold promise for new efficiencies in vehicles and other structural systems. Here we examine the possibility of integrating three functions into a structural system by combining the functions of energy harvesting, self-sensing and reduced energy control into a composite structure. The composite considered here is a sandwiched material with the hope that future research will include a more integrated composite. Each functionality is described in detail and structural modeling results are presented. The motivating application is the wing spar of a UAV with the goal of providing self-contained vibration suppression and gust alleviation. The layered components consist of: the fiberglass spar, a thin film battery, piezoceramic wafers, a flexible solar array and an electronics module as illustrated in Fig. 1.

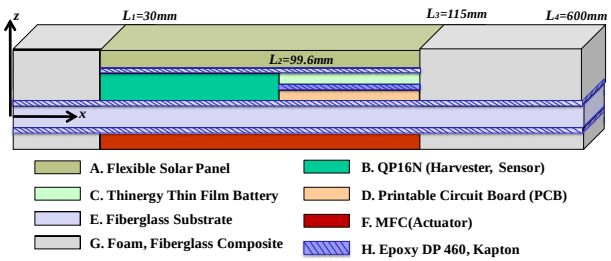

Fig.1. Schematic of multifunctional sandwich composite wing showing the various functionalities.

The key issues in researching the possible usefulness of such an approach are 1) how much energy can be harvested, and 2) is harvested energy enough to effectuate active control. Certainly, passive control can be achieved through aero-elastic harvesting as shown in [1] through passive means (shunt damping). Here we focus on active reduced energy control and look for the controller that uses the minimum amount of energy [2]. Also key importance is the weight added and in that context does such an approach make sense [3].

This work builds off of our previous research in self-charging structures [4]. A small prototype of the motivating device is illustrated in Fig. 2. This multifunctional wing spar consists of collocated self-powering and self-sensing functionalities, as well as simultaneous energy harvesting and gust alleviation abilities.

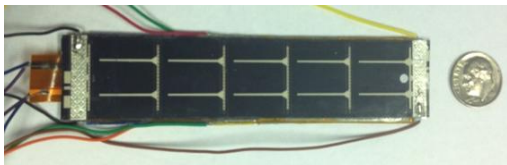

Fig. 2. A sandwich composite spar with solar panel, piezoelectric and thin film battery materials.

The basic concept is that the wing vibrates some during normal flight under normal conditions. These vibrations along with any available sunlight are harvested. When the wing experiences a strong, unexpected aerodynamic load (gust) the spar will sense the increased vibration levels and provide active control to reduce the vibration and help maintain stability.

2 Components

The structural functionality (Fig.1) is a UAV multifunctional wing spar, designed to fit in the polystyrene insulating foam (G) core wrapped in fiberglass substrate (E), for lightweight and strength purposes. The PZT harvester/sensor (B) layered on the top surface of the fiberglass substrate uses monolithic PZT (QuickPack QP10n). The Micro-Fiber Composite MFC 8528 P1 is the PZT actuator (F) layered on the bottom surface of the fiberglass substrate. The MFC was recently developed in the NASA Langley Research Center [5]. Due to its high actuating authority, the *d33* effect P1 type MFCs are commonly used as PZT actuators. The thin film

battery (C) (Thinergy MEC-1017SES batteries) allows for power storage from harvesting as well as for energy supply for wind gust alleviation. The electronics module combines energy harvesting conditioning, sensing circuitry, and the optimal vibration controller discussed below on a single layer of Printable Circuit Board (PCB). These multifunctional layers, together with the foam core, form the multi-layer wing spar. 3M ScotchWeld™ DP460 epoxy, bracketed by Kapton, is used in the individual layer layup. Both are grouped together as layer H. The wing spar geometric and material properties are given in Table 1.

Table 1. Geometric and Material Properties of Multifunctional Wing Spar.

Layer	Length (mm)	Width(mm)	Thickness (mm)	Mass (g)	Young's Module (GPa)
Solar Panel	85	28	0.2	0.69	52
QP10N	59.6	25.4	0.38	2.25	67
Battery	25.4	25.4	0.18	0.46	55
PCB	25.4	25.4	0.20	0.23	60
Fiberglass Substrate	735	28	10	185.2	71
MFC	85	28	0.18	2.92	63
Foam, Fiberglass composite	650	28	0.76	4.10	60
3D Epoxy	1580	28	0.008	0.35	3
Kapton	1580	28	0.0075	0.41	3.7

3 Electromechanical Euler-Bernoulli Modeling

The absolute transverse displacement of the wing spar at any point x and time t is given by:

$$w(x,t) = w_b(x,t) + w_{rel}(x,t), \tag{1}$$

where $w_b(x,t)$ and $w_{rel}(x,t)$ stand for the base and relative transverse displacement of the wing spar. The relative vibration response can be represented as finite series expansion of admissible trial functions $\Phi_r(x)$ and unknown modal coordinates $\eta_r(t)$:

$$w_{rel}(x,t) = \sum_{r=1}^{N} \Phi_r(x)\eta_r(t), \tag{2}$$

where N is the truncation order of the series. The admissible trial function $\Phi_r(x)$ has to satisfy the above boundary conditions. In order to avoid hyperbolic eigenfunction forms, a simple admissible trial function is adopted here, which is typically used for long, thin cantilever beams [6]:

$$\Phi_r = 1 - \cos\left(\frac{(2r-1)\pi x}{2L}\right). \tag{3}$$

For the considered multifunctional electromechanical wing spar, the extended Hamilton's principle over a given time period satisfies the following relation in terms of kinetic T, potential energy U, internal energy E_{ie} and non-conservative energy E_{nc}:

$$\delta\int_{t_1}^{t_2} (T - U + E_{ie} + E_{nc})dt = 0. \tag{4}$$

The electromechanical energy follows the Euler-Lagrange Equations:

$$\frac{d}{dt}\frac{\partial T}{\partial \dot{q}} = \frac{\partial T}{\partial q} - \frac{\partial U}{\partial q} + \frac{\partial E_{ie}}{\partial q} + \frac{\partial E_{nc}}{\partial q}, q = \eta_i(t), v_i(t). \tag{5}$$

Substituting the assumed mode solutions into the kinetic, potential and internal energy terms yields:

$$U^{o,a} = \frac{1}{2}\sum_{i,l=1}^{N}[\eta_i(t)\eta_l(t)k_{il}^{o,a} - \eta_i(t)v^{o,a}(t)\theta_i^{o,a}]; \tag{6}$$

$$\begin{aligned} T^{o,a} = {} & \frac{1}{2}\sum_{i,l=1}^{N}(\dot{\eta}_i(t)\dot{\eta}_l(t)m_{il}^{o,a} + 2\dot{\eta}_i(t)\int_0^{L4}\rho A_s(x)\Phi_i\frac{\partial w_b}{\partial t}dx) \\ & + \frac{1}{2}\int_0^{L4}\rho A_s(x)\left(\frac{\partial w_b}{\partial t}\right)^2 dx; \end{aligned} \tag{7}$$

$$E_{ie}^{o,a} = \frac{1}{2}\sum_{i=1}^{N}(\eta_i v^{o,a}\theta_i^{o,a} + C_p^{o,a}v^{o,a}). \tag{8}$$

Here ρ, A_s, v are the global density, the cross section area of the wing spar, and the voltage across the PZT electrodes. Here, the superscripts o, a, denote the output (harvesting/sensing) and the actuation PZT layers. The subscripts s, p represent the wing spar structure and PZT layer, respectively.

The mass and stiffness components are defined as:

$$m_{il} = \int_0^{L4}\rho A_s(x)\Phi_i\Phi_l dx, \tag{9}$$

$$k_{il}^{o,a} = \int_0^{L4} E_s I_s \Phi_i''\Phi_l'' dx + \int_{L1}^{L2L3} E_{31,33}^{E} I_p^{o,a}\Phi_i''\Phi_l'' dx. \tag{10}$$

Here E, I denote Young's modulus and the second moment of inertia, respectively. Note that an over-dot stands for ordinary differentiation with respect to the temporal variable t, and a prime denotes ordinary differentiation with respect to the spatial variable x. The coupling coefficient is defined as:

$$\theta_{ie}^{o,a} = \int_{L1}^{L2,L3} J_p^{o,a}\Phi_i'' dx. \tag{11}$$

The coupling terms J_p of the output (harvesting/sensing) PZT and actuation PZT are defined as:

$$J_p^o = \iint_{po} z \frac{d_{31}E_{31}^E}{h_{po}} dydz, J_p^a = \iint_{pa} z \frac{d_{33}E_{33}^E}{h_{pa}} dydz. \quad (12)$$

Here h_{pa} and h_{po} represent the thickness of the output (harvesting/sensing) PZT and actuation PZT, respectively. The capacitance term C_p of the output (harvesting/sensing) PZT and the actuation PZT is defined as:

$$C_p^o = \frac{\varepsilon_{31}^s A_p^o}{h_{po}}, C_p^a = \frac{\varepsilon_{33}^{s*} A_p^a}{h_{pa}}. \quad (13)$$

Here ε^s is the permittivity constant at constant mechanical strain field, A_p^o, A_p^a denote the electrode surface area of the output (harvesting/sensing) and the actuation PZT layers. The non-conservative work is due to the harvesting/sensing PZT output energy and/or the PZT actuation energy:

$$E_{nc}^{o,a} = Q^{o,a}(t)v^{o,a}(t). \quad (14)$$

Here $Q^{o,a}$ denotes the output charge or actuation charge of the PZT harvester or actuator.

3.2 Harvesting Characteristics and Self-sensing Abilities by Solving Electromechanical Euler-Lagrange Equations

The ambient normal vibration source from small UAVs produces a continuous charge output, which is stored in the thin film battery. A voltage signal read from a parallel connected resistor is used to analyze both harvesting characteristics and sensing ability. Those analytical equations are derived in this section. After substituting each energy terms back into the Euler-Lagrange Equations resulting from (5), one obtains:

$$\sum_{l=1}^{N} m_{il}\ddot{\eta}_l + k_{il}\eta_l - \theta_i^o v_i^o - f_i = 0,$$
$$C_p^o \dot{v}^o + \frac{v^o}{Z^o} + \sum_{i=1}^{N}(\theta_i^o \dot{\eta}_i^o) = 0. \quad (15)$$

Here the Z^o denotes the impedance of the output circuit (pure resistance in this case). The forcing f_i due to the base excitation is given by:

$$f_i = -\int_0^L \rho A_s(x)\Phi_i(x)\frac{\partial^2 w_b}{\partial t^2}dx. \quad (16)$$

After introducing the damping components and rewriting the equivalent Euler-Lagrange equations (15) in matrix form, one obtains:

$$\mathbf{M}\ddot{\boldsymbol{\eta}} + \mathbf{C}\dot{\boldsymbol{\eta}} + \mathbf{K}\boldsymbol{\eta} = \mathbf{f} + \theta^o \mathbf{v}^o, \quad (17)$$

$$C_p^o \dot{\mathbf{v}}^o + \frac{\mathbf{v}^o}{Z^o} + \theta^o \dot{\boldsymbol{\eta}}^o = 0. \quad (18)$$

Rayleigh damping for nonlinear incremental analysis is used for this study:

$$\mathbf{C} = \kappa\mathbf{M} + \gamma\mathbf{K} = 1.34\mathbf{M} + 1.89e^{-7}\mathbf{K}. \quad (19)$$

The coefficients κ and γ are determined using the damping ratios associated with the 1st and 2nd modes, 0.37% and 0.1% respectively. The damping matrix must satisfy the following properties in order to uncouple the modal equations:

$$2\omega_{ni}\zeta_i = \Phi_i^T \mathbf{C}\Phi_i = \kappa + \gamma\omega_{ni}^2. \quad (20)$$

Here ω_{ni} and ζ_i represent the ith eigen-frequency and its associated damping ratio. Assuming the ambient vibration working on the clamped end of the wing spar source has a harmonic form, the wing vibration base acceleration and the forcing vector will have a harmonic form as well, given by:

$$w_b(t) = w_b e^{j\omega t}, a_b(t) = a_b e^{j\omega t}, f_i(t) = -m_i a_b e^{j\omega t}. \quad (21)$$

The harmonic forcing excitation leads to a harmonic solution for the generalized coordinates and the voltage, of the form:

$$\boldsymbol{\eta}(t) = \boldsymbol{\eta}e^{j\omega t}, v(t) = Ve^{j\omega t}. \quad (22)$$

The steady-state forms of Equations (17) and (18) then become:

$$(-\omega^2\mathbf{M} + j\omega\mathbf{C} + \mathbf{K})\boldsymbol{\eta}^o = \mathbf{f} + \boldsymbol{\theta}^o V^o, \quad (23)$$

$$(j\omega C_p^o + \frac{1}{Z^o})V^o + j\omega\boldsymbol{\theta}^o\boldsymbol{\eta}^o = 0. \quad (24)$$

The steady-state solutions are then given by:

$$V^o = \frac{-j\omega\boldsymbol{\theta}^{oT}\boldsymbol{\eta}^o}{j\omega C_p^o + \frac{1}{Z^o}}, \quad (25)$$

$$\boldsymbol{\eta}^o = (-\omega^2\mathbf{M} + j\omega\mathbf{C} + \mathbf{K} + \frac{-j\omega\boldsymbol{\theta}^o\boldsymbol{\theta}^{oT}}{j\omega C_p^o + \frac{1}{Z^o}})^{-1}\mathbf{f}. \quad (26)$$

Here the superscript T stands for transpose. The steady-state solutions lead to the output harvesting voltage-to-base acceleration FRF:

$$\frac{v^o(t)}{a_f e^{j\omega t}} = \frac{j\omega\boldsymbol{\theta}^{oT}}{j\omega C_p^o + \frac{1}{Z^o}}(-\omega^2\mathbf{M} + j\omega\mathbf{C} + \mathbf{K} + \frac{-j\omega\boldsymbol{\theta}^o\boldsymbol{\theta}^{oT}}{j\omega C_p^o + \frac{1}{Z^o}})^{-1}\mathbf{M}. \quad (27)$$

The ambient normal wing vibration is simulated with 0.2g RMS acceleration over a frequency bandwidth of 5Hz ~ 300Hz. An optimal resistance of 100kOhm is found to maximize the harvested power efficiency. The harvested voltage to base acceleration FRF for

the first two modes is presented in Fig.3 at this optimal load resistance. The assumed modes formulation is truncated at order fifty to ensure the convergence of the first two modes.

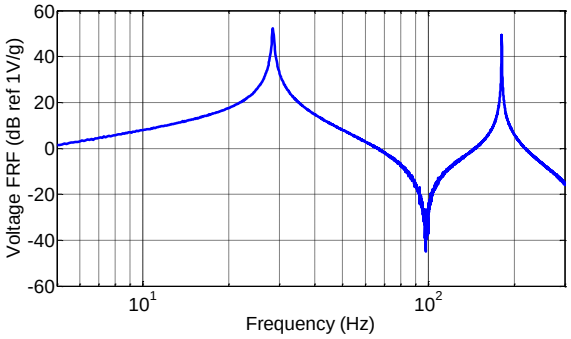

Fig.3. Harvested voltage to base acceleration FRF for a 100kOhm optimal load resistance.

The instantaneous harvested power for a 100kOhm optimal resistant load is plotted in Fig.4.

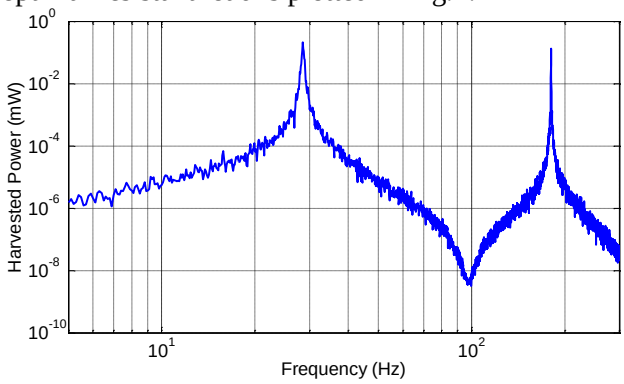

Fig.4. Harvested power spectrum for 100kOhm optimal load resistance.

Fig.5 compares the displacement to base acceleration frequency response function (FRF) using analytical and FEM modeling. The base acceleration is represented in terms of the acceleration of gravity, g = 9.81 m/s^2. The bending stiffness of each longitudinal section is estimated by means of the rule of mixtures (ROM) [7] and the cross section transformation (CST) [8]. Both of them are implemented for modal frequency predictions using analytical and FEM modeling. The ROM and CST models are in perfect agreement, for both analytical and FEM modeling. The analytical models are within 5% root mean square (RMS) error of the FEM models.

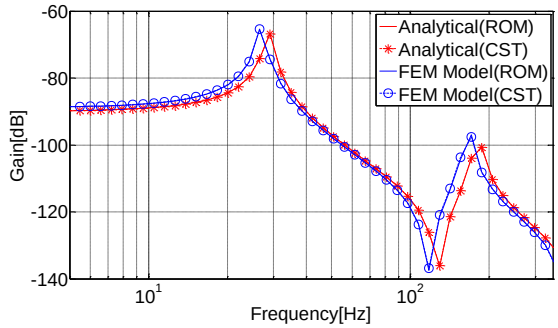

Fig.5. Modal frequency prediction using both analytical and FEM modeling.

If one defines the self-sensing sensitivity as the derivative of the sensing voltage v^s with respect to the PZT covered strain S^s_{xx}, the following relations can be derived from equation (19):

$$\frac{\partial v^s}{\partial S^s_{xx}} = \frac{h^s_y d_{31} E^E_{31}}{C^o_p} = \frac{d_{31} E^E_{31} h^o_p}{\varepsilon^s_{31} h^s_x}. \tag{29}$$

Here, h^s_y and h^s_x denote the width and the length of the piezoelectric sensor, respectively. Note that the current flow into the sensor is neglected since the impedance is very high (100kOhm, equivalent to open circuit conditions). Fig.6 presents the voltage sensitivities of the self-sensing bending strain sensor in frequency domain.

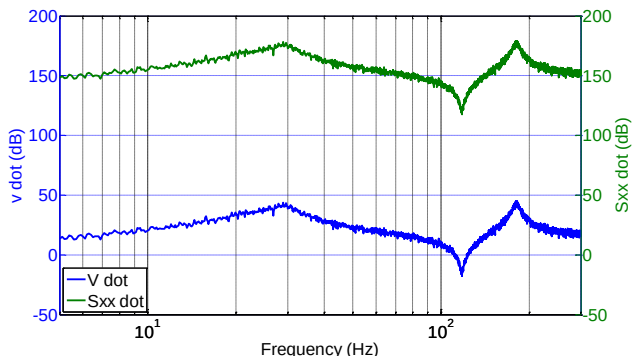

Fig.6. Spectrums of sensing voltage and bending strain time derivatives.

4 Simultaneous Energy Harvesting and Vibration Control

In order to generate the clear sky normal wing vibration and cumulus cloud wind gust signals with the required intensity, scale lengths and PSD functions for a given flight velocity and height, a Gaussian white noise source $n(t)$ ~ N(0,1) with PSD function of 1, is amplified by a wind gust gain K_g and filtered by a wind gust transfer function $G_v(s)$:

$$K_g = \sqrt{\frac{3\sigma_v^2 U_0}{\pi L_v}}, G_v(s) = \frac{s + \frac{U_0}{\sqrt{3}L_v}}{(s + \frac{U_0}{L_v})^2}.$$

Fig.7 shows an example of simulated clear sky normal wing vibration and cumulus cloud wind gust signals, in acceleration units.

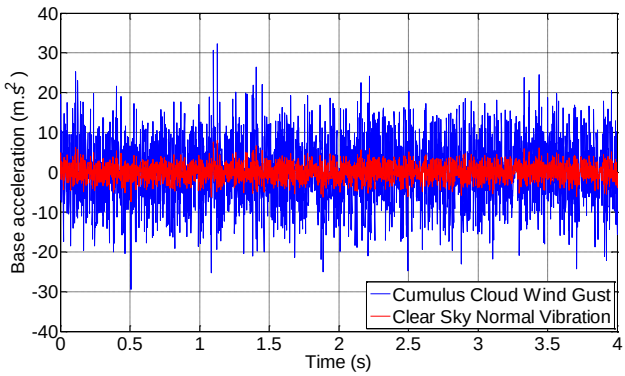

Fig.7. Normal Wing Vibration and Wind Gust Acting on Multifunctional Wing Spar Base, with U_0=15m/s, L_v=350m.

Our previous experimental validated results show a 67% energy reduction when using on-off switching reduced energy control laws for transient vibration control [9], compared to conventional nonlinear control laws. The governing equation of the multifunctional wing spar yields:

$$\mathbf{M}\ddot{\boldsymbol{\eta}} + \mathbf{C}\dot{\boldsymbol{\eta}} + \mathbf{K}\boldsymbol{\eta} = \mathbf{f} + \boldsymbol{\theta}^s V^s + \boldsymbol{\theta}^a V^a, \quad (30)$$

$$C_p^s \dot{V}^s + i^S + \boldsymbol{\theta}^s \dot{\boldsymbol{\eta}}^s = 0. \quad (31)$$

$$C_p^a \dot{V}^a + i^a + \boldsymbol{\theta}^a \dot{\boldsymbol{\eta}}^a = 0. \quad (32)$$

Here i^S denotes the current flowing through the sensor, and i^a denotes the current flowing through the actuator, which depends on the feedback control algorithm and on the load impedance. The reduced energy control laws produce a nonlinear switching logic by saturating the actuating voltage generated by the PSF controller. The PSF control algorithm takes the same transfer function as the positive position feedback control law [10], which is driven by a PSF op-amp and a voltage buffer op-amp:

$$\frac{v_o}{v_i} = k \frac{\frac{1}{\tau_1 \tau_2}}{s^2 + s\frac{1}{\tau_2} + \frac{1}{\tau_1 \tau_2}}. \quad (33)$$

Here the gain and time coefficient are defined as:

$$k = \frac{R_2}{R_1}(1 + \frac{R_5}{R_4}), \tau_1 = R_2 C_1, \tau_2 = R_3 C_2. \quad (34)$$

Upon encountering the cumulus cloud disturbance shown in Figure 8, the reduced energy control laws yield 13 dB cumulative reduction in the 5Hz~300Hz frequency bandwidth, as seen in Fig.8. The cumulative displacement for one given frequency bin is the sum of the displacement over all preceding frequency bins. In this paper, enhanced Positive Strain Feedback (PSF) reduced energy control are developed for gust alleviation over the first two natural frequencies, using the energy harvested from ambient normal wing vibrations.

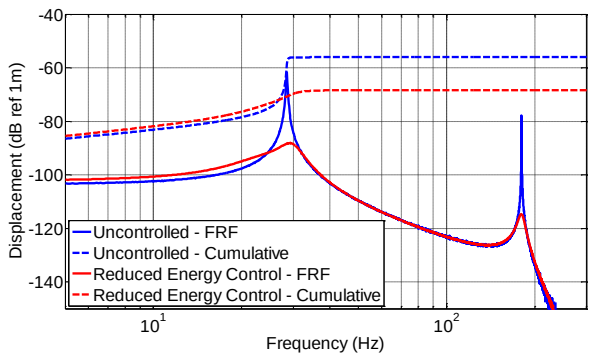

Fig.8. Wind Gust Disturbed Tip Displacement Spectrums of Multifunctional Wing Spar Before and After Reduced Energy Control.

In time domain, the wing spar tip displacement RMS value is reduced from 1.6 mm down to 0.35 mm. The maximum tip displacement is reduced from ±4.5 mm down to ±1.0 mm, as seen in Fig.9.

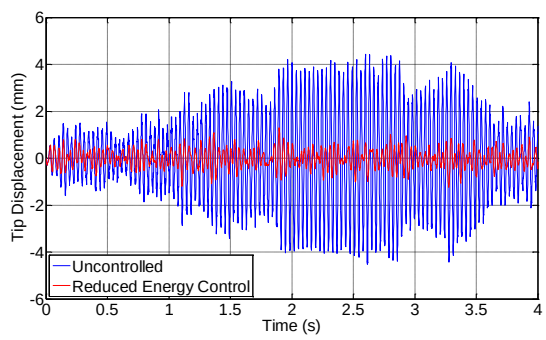

Fig.9. Disturbed wing spar tip response in time domain before and after reduced energy control.

The real part and the imaginary part of the cross-spectrum between instantaneous voltage and current represent the active and reactive power associated with a given component, respectively. The unit of reactive power is volt-ampere reactive (var). The active, reactive and apparent power associated with

the sensor, actuator and harvester are detailed in Table 2. The apparent control power required for 13dB reduction in tip displacement is 6.42mW, which is 40 times higher than the harvesting power of 0.16mW. That is, in order to control a 1 minute long cumulus gust, 40 minutes of harvesting are needed.

Table 2. Power Associated With Each Electric Component.

Electric Element	Active Power (mW)	Reactive Power (mVAr)	Apparent Power (mVA)
Sensor	0.01	0.00	0.01
Actuator	6.42	4.94	8.63
Harvester	0.16	0.00	0.16

5 Conclusions

A novel multifunctional composite structure for simultaneous energy harvesting and gust alleviation is investigated in this paper. A recently developed on-off switching reduced energy control law is implemented to reduce control power while preserving control performance. The multifunctional composite wing spar is designed to be compatible with collocated self-harvesting, self-sensing and self-control functionalities using piezoelectric materials. Numerical simulations show that the tip displacement due to an unexpected wind gust disturbance can be reduced by 13dB, using vibration energy harvested during a period of time at least 40 times longer than the wind gust duration.

6 Acknowledgement

The authors gratefully acknowledge the support of Air Force Office of Scientific Research (AFOSR) Grant Number FA9550-09-1-0625 "Simultaneous Vibration Suppression and Energy Harvesting" under the direction of "Les" Lee.

6 References

[1] C. De Marqui Jr.; W. Vieira; A. Erturk; D.J. Inman, "Modeling and Analysis of Piezoelectric Energy Harvesting from Aeroelastic Vibrations Using the Doublet-Lattice Method," *Transactions of the ASME. Journal of Vibration and Acoustics*, 133, 9. 2011.

[2] Y. Wang; D.J. Inman, "Comparison of Control Laws for Vibration Suppression Based on Energy Consumption," *Journal of Intelligent Material Systems and Structures.*, 2011.

[3] M. Qidwai; J. Thomas; W. Poque III, Structure-battery Composites for UUVs: Multifunctional Interaction Effects, In AIAA/ASME/SAE 50th Structures, Structural Dynamics and Materials Conference, 4-7 May 2009, Palm Springs, CA, USA, 2009; p 2314.

[4] S.R. Anton; A. Erturk; D.J. Inman, "Multifunctional self-charging structures using piezoceramics and thin-film batteries," *Smart Materials and Structures*, 19, 115021 (15 pp.). 2010.

[5] W.K. Wilkie; R.G. Bryant; J.W. High; R.L. Fox; R.F. Hellbaum; A. Jalink Jr.; B.D. Little; P.H. Mirick, Low-cost Piezocomposite Actuator for Structural Control Applications, In Proceedings of SPIE, the International Society for Optical Engineering, Smart Structures and Materials, 6-8 March 2011, Newport Beach, CA,USA, 2000; Vol. 3991, pp 323.

[6] L. Meirovitch, "*Fundamentals of Vibrations*", McGraw-Hill: Boston, 2001.

[7] R.M. Jones, "*Mechanics of composite materials*", Scripta Book Co.: Washington, 1975.

[8] M. Vable, "*Mechanics of materials*", Oxford University Press: New York, 2002.

[9] Y. Wang; D.J. Inman, Energy-based Comparison of Various Controllers for Vibration Suppression Using Piezoceramics, In Proceedings of SPIE, the International Society for Optical Engineering, 4-7 March 2011, San Diego, CA,USA, 2011; Vol. 7977.

[10] Y. Wang; D.J. Inman, Theoretical and Experimental Comparison of Two Controllers for Vibration Suppression with Minimum Energy, In AIAA/ASME/SAE 52nd Structures, Structural Dynamics and Materials Conference, 7-11 April 2011, Denver, CO, USA, 2011; pp 75.